ACS APPLIED MATERIALS & INTERFACES

www.acsami.org

Research Article

Designing Triangular Silver Nanoplates with GSH/GSSG Surface Mixed States as Novel Nanoparticle-based Redox Mediators for Electrochemical Biosensing

Liu Qu,[§] Jingshuai Li,[§] Yu Du,* Lei Yang, Xiang Ren, Lei Liu, Xuejing Liu, Yuyang Li, and Qin Wei

Cite This: *ACS Appl. Mater. Interfaces* 2022, 14, 26271−26278

Read Online

ACCESS | Metrics & More | Article Recommendations | Supporting Information

ABSTRACT: Herein, a dual signal-quenched electrochemical (EC) biosensing strategy utilizing surface-engineered trisodium citrate (TSC)−glutathione (GSH)/oxidized glutathione (GSSG)-capped triangular silver nanoplates (Tri-Ag $NPs_{TSC-GSH/GSSG}$) as a novel nanoparticle-based redox mediator was explored for biomarker determination. In contrast with conventional redox mediators, Tri-Ag $NPs_{TSC-GSH/GSSG}$ provided more admirable EC performance along with a lower oxidation potential (~0.14 V). Taking advantage of the split-type mode, the immune response in a 96-well microplate was independent from EC detection, which could effectively eliminate the biological interference and thereby greatly enhance the sensitivity. As for the surface engineering process of Tri-Ag NPs, it was composed of partial GSH replacement and the formation of the GSH/GSSG surface mixed state. Primarily, the signal response of Ag $NPs_{TSC-GSH}$ decreased due to the hindrance of GSH on electron transfer. Moreover, varying proportions of GSH/GSSG could further impede the oxidation process of Tri-Ag $NPs_{TSC-GSH/GSSG}$ and eventually realize efficient dual signal quenching of this system. Notably, the ZIF-67@MIL-88B-GO_x nanocomposite as the label was applied for a cascade reaction system with GSH peroxidase-like activities to form the optimal GSH/GSSG proportion, causing sensitive changes in signal response with a range of different antigen concentrations. On this basis, the fabricated biosensor provided measurable outputs of aflatoxin B1 concentrations in a linear range of 0.0005−50 ng/mL with a low detection limit of 0.61 pg/mL (S/N = 3). All of the results indicated that the novel biosensor could be a promising analytical tool for future biomarker detection.

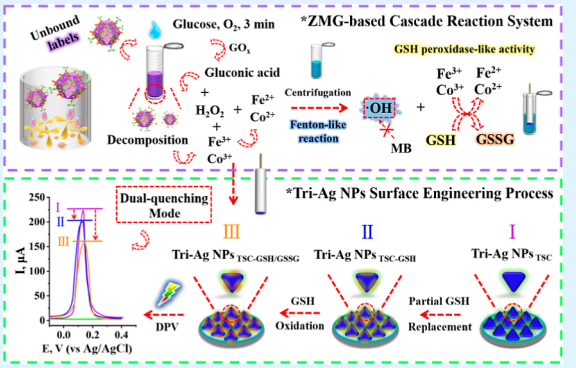

KEYWORDS: *novel nanoparticle-based redox mediators design, surface-engineered Tri-Ag NPs, split-type mode, ZIF-67@MIL-88B-GO_x-based cascade reaction, aflatoxin B1*

INTRODUCTION

Presently, electrochemical (EC) biosensors as an efficient instrument have exerted crucial function for trace biomolecules analysis in clinical diagnosis.[1−3] In regard to the overall biosensor construction, a novel split-type mode which separates specific recognition from an EC detection device could effectively eliminate the biological interference on a single electrode.[4−6] As for the redox-based EC biosensor,[7,8] designing a nanoparticle redox mediator (NRM)-based bioassay method with less EC interference, wider EC windows, and higher efficiency and sensitivity has become increasingly desirable. As far as we know, the NRM-based EC biosensor has been rarely reported. Whereas, Zou's group initially developed trisodium citrate (TSC)−glutathione (GSH)-capped triangular silver nanoplates (Tri-Ag $NPs_{TSC-GSH}$) as the efficient NRMs for GSH EC sensing analysis, which exhibited higher selectivity and lower oxidative potential than traditional RMs.[9] What is more, the existence of a redox couple with intrinsic GSH peroxidase-like activity such as Fe^{3+}/Fe^{2+} and so forth could convert GSH into oxidized glutathione (GSSG).[10,11] Inspired by the abovementioned ideas, a ZIF-67@MIL-88B-GO_x (ZMG)-based cascade reaction system with various oxidation capacities for GSH has been proposed. After the engineering process, the Tri-Ag $NPs_{TSC-GSH/GSSG}$ is designed as a novel NRM, applying for sensitive EC sensing that combined with the split-type mode for fabricating biosensors in this work.

Different morphologies such as rods, spheres, wires, triangular plates, and so forth of Ag nanoparticles determine their various intrinsic properties.[12−14] Especially, Tri-Ag NPs with unique optical and EC properties have become reliable candidates for application in catalytic, sensing, and other fields.[15−17] For instance, using melamine as a protective agent

Received: April 3, 2022
Accepted: May 19, 2022
Published: May 27, 2022

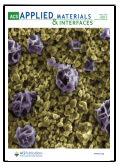

Scheme 1. Schematic Illustration of the (A) Synthetic Approach of ZMG Labels, (B) Preparation of the ZMG-Based Cascade Reaction System, (C) Surface Engineering Mechanism of Surface-Confined Tri-Ag NPs_{TSC} and Fabrication Process of This Biosensor

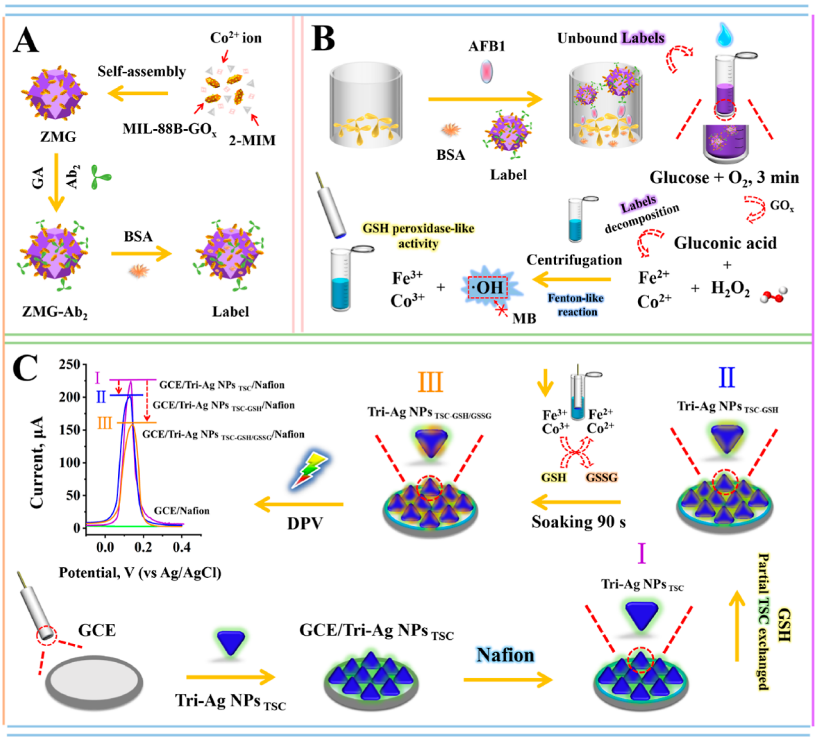

for sodium 4-vinylbenzenesulfonate-etched Tri-Ag NPs, different localized surface plasmon resonance properties were obtained for novel melamine sensing.[18] Using the Tri-Ag NPs_{TSC} that was prepared through a direct chemical reduction method for the electrocatalytic reduction of CO_2 to CO.[19] As for Tri-Ag NPs_{TSC}, the surface-capped TSC could be replaced by GSH thiol in part to initiate the surface engineering of Tri-Ag NPs. Besides, GSH could be oxidized into GSSG to form GSH/GSSG surface mixed state-capped Tri-Ag NPs. Through the abovementioned method, the EC communication between targets and electrodes could be effectively facilitated. The surface-engineered Tri-Ag NPs exhibit acceptable EC performance with a low oxidative potential located at ~0.14 V. Thus, it endows Tri-Ag $NPs_{TSC-GSH/GSSG}$ with the promising possibility of being incorporated into NRM-based biosensing.

Although the hybrid metal−organic framework (MOF) which incorporates MIL-88B (the Fe-based MOF) nanorods into a ZIF-67 crystal (ZIF-67@MIL-88B) was designed as the precursor of advanced electrode materials with outstanding performance.[20] Whereas, novel structures and tailored compositions could make it highly desirable for the biosensing field. In particular, on the one hand, the ZIF-67@MIL-88B composite exhibits inherent peroxidase-mimic activity.[21,22] On the other hand, GO_x could be loaded onto the surface of MIL-88B to synthesize MIL-88B-GO_x via coordination adsorption.[23] Notably, the GO_x-catalyzed oxidation of glucose could generate gluconic acid and H_2O_2, which could initiate the overall cascade reactions.[24] Furthermore, the released Fe^{3+}/Fe^{2+} and Co^{3+}/Co^{2+} redox couples are favorable candidates for realizing GSH oxidation. As a consequence, ZMG comes into being through the self-assembly process (Scheme 1A). Also, it is involved in the ZMG-based cascade reaction system (Scheme 1B) for designing the surface-engineered Tri-Ag $NPs_{TSC-GSH/GSSG}$ NRMs.

As shown in Scheme 1B, after incubating Ab_1, bovine serum albumin (BSA), antigen, and ZMG-Ab_2 solution in a 96-well microplate, the immune incubation of the split-type biosensor was completed. Subsequently, different quantities of the unbound ZMG-Ab_2 bioconjugate were applied to the cascade reaction system with varying GSH peroxidase-like activities. As depicted in Scheme 1C(a), the Tri-Ag NP-involved sensing interface has been fabricated successfully. Herein, dual signal quenching of Tri-Ag NPs could be realized through partial GSH replacement and the formation of a GSH/GSSG mixed state on their surface. In particular, varying proportions of GSH/GSSG surface mixed states exhibited different degrees of hindrance to the oxidation process of Tri-Ag $NPs_{TSC-GSH/GSSG}$. Causing sensitive changes in differential pulse voltammetry (DPV) response with a range of different antigen concentrations. Hence, the split-type immunoassay was realized. As for the split-type mode, separating the sandwich-type immunoassay from EC sensing could effectively avoid complex steric hindrance and immune interference at a single EC sensing interface.[5,25,26] Thus, a more efficient EC response could be obtained. Besides, applying the Tri-Ag $NPs_{TSC-GSH/GSSG}$ NRMs to construct the sensing interface could acquire excellent EC response under a low oxidation potential. In combination with the abovementioned advantages, the split-type surface-engineered Tri-Ag NP-involved biosensor with high sensitivity and satisfying properties is employed for the biosensing of aflatoxin B1 (AFB1). One of the most toxic mycotoxin, causing significant health risk and damage to humans and animals.[27,28] Eventually, a low limit of detection (LOD) of 0.61 pg/mL is calculated for the AFB1 real antigen target analysis. Convincing the prominent application potential of the proposed biosensor

https://doi.org/10.1021/acsami.2c05869
ACS Appl. Mater. Interfaces 2022, 14, 26271−26278

for sensitive, facile, and efficient analysis of trace biomarkers in complex serum samples.

EXPERIMENTAL SECTION

Preparation of Tri-Ag NPs$_{TSC}$. For the synthesis procedure of Tri-Ag NPs$_{TSC}$, typical steps reported by Liu's group have been referred to.[19] Primarily, a drop of $NaBH_4$ (0.1 mol/L, 250 μL) was rapidly injected into an as-prepared 24.75 mL of the homogeneous solution containing $AgNO_3$ (0.05 mol/L, 50 μL), TSC (0.075 mol/L, 500 μL), and H_2O_2 (30 wt %, 60 μL) to trigger the reduction reaction. After several minutes, the yellow colloidal solution passed from light to dark, which means the formation of small Ag nanoparticles. Within the next few seconds of changing from red to green, the solution color ultimately turned to jewelry blue, manifesting that the Tri-Ag NPs$_{TSC}$ was synthesized successfully. Finally, the obtained product was washed, redispersed in ultrapure water, and stored at 4 °C for further use.

Preparation of the ZMG Composites. The synthesis approach of polyvinylpyrrolidone (PVP)-functionalized MIL-88B-GO$_x$ is shown in the Supporting Information. The ZMG composites were prepared by referring to Zhang's work with some modification.[20] The specific process is shown in Scheme 1A. In brief, a 2-methylimidazole solution (0.08 mmol/L, 5 mL) was added rapidly into an aqueous solution combining Co $(NO_3)_2{\cdot}6H_2O$ (0.02 mmol/L, 3 mL) and PVP-functionalized MIL-88B-GO$_x$ nanorod suspension (0.8 mL) under magnetic stirring. Subsequently, the abovementioned mixture was left to age at 24 °C for 6 h. Finally, the product was collected by centrifugation, washed several times with methanol, and dried at room temperature.

Preparation of the ZMG-Ab$_2$ Bioconjugate. The as-prepared ZMG dispersed solution (1.6 mg/mL, 1 mL) was primarily mixed thoroughly with the glutaraldehyde solution (0.5 wt %, 500 μL) with the following stirring for 3 h. Then, the abovementioned solution was added to the AFB1-Ab$_2$ solution (10 μg/mL, 500 μL) and kept shaking at 4 °C for 6 h. After centrifuging and washing, nonspecific active sites of the obtained bioconjugate were blocked by incubation with BSA, then redispersed into the phosphate-buffered saline (PBS) solution (pH 7.4, 1 mL) and stored at 4 °C.

Preparation of the ZMG-based Cascade Reaction System. As exhibited in Scheme 1B, for the procedure of immunoassay, AFB1−Ab$_1$ solution (10 μg/mL, 50 μL), BSA solution (0.1% wt, 50 μL), varying concentrations of target AFB1 (500 fg/mL to 50 ng/mL, 50 μL), and the prepared ZMG-Ab$_2$ bioconjugate (1.6 mg/mL, 50 μL) were incubated in a 96-well microplate in sequence. The microplate was rinsed with the PBS solution after each incubation step. For the ZMG-based cascade reaction system, first the unbound ZMG-Ab$_2$ labels were transferred into a centrifuge tube. Subsequently, a drop of the glucose solution (0.05 mmol/L, 50 μL) was injected and generated gluconic acid and H_2O_2 that initiated the ZMG-based cascade reaction. After reacting for 3 min, the abovementioned mixture was centrifuged to terminate the production of H_2O_2, then methylene blue (MB) was added as a trapping agent to remove $^{\bullet}OH$, and the supernate was ultimately left for further use.

Assembly Process of the Designed NRM-involved EC Sensing Interface (Tri-Ag NPs$_{TSC}$ as the Initial NRMs). A detailed assembly procedure of the glassy carbon electrode (GCE)/Tri-Ag NPs$_{TSC-GSH/GSSG}$/Nafion EC sensing interface is presented in Scheme 1C. First, 6 μL of the as-prepared Tri-Ag NPs$_{TSC}$ was modified onto a polished GCE with the following immobilized by Nafion film (0.05% wt, 8 μL) to obtain GCE/Tri-Ag NPs$_{TSC}$/Nafion. As for the surface engineering procedure, subsequently, a drop of the GSH solution (500 pmol/L, 8 μL) was added to the above modified electrode for partial thiol exchange (10 min) to form GCE/Tri-Ag NPs$_{TSC-GSH}$/Nafion. Furthermore, referring to the ZMG-based cascade reaction system, the prepared electrode was soaked in a supernate with varying degrees of GSH peroxidase-like activity for 90 s to oxidize GSH to GSSG. Finally, the designed Tri-Ag NPs$_{TSC-GSH/GSSG}$ NRM-involved working electrode was assembled successfully, then washed and dried under a N_2 atmosphere for further EC measurement.

EC Measurement Section. For the determination of the AFB1 biomarker, the DPV method was implemented to measure the DPV response of the designed NRM-involved working electrode. A 0.1 mol/L pH 7.4 Tris-HCl buffer solution was used as the base solution with the DPV signal being recorded from −0.1 to 0.4 V. Obviously, a series of measured DPV responses of surface-engineered Tri-Ag NPs$_{TSC-GSH/GSSG}$ were essentially relevant to AFB1 with various concentrations.

RESULTS AND DISCUSSION

Morphology, Structural, and Optics Characterization of Ag NPs$_{TSC}$. Primarily, main diffraction peaks of the X-ray diffraction (XRD) patterns at 2θ = 38.1, 44.3, 64.4, and 77.5° are well correspond to the (111), (200), (220), and (311) planes of Ag NP crystals (Figure S1), respectively. As shown in Figure 1A,B, high-resolution transmission electron microscopy

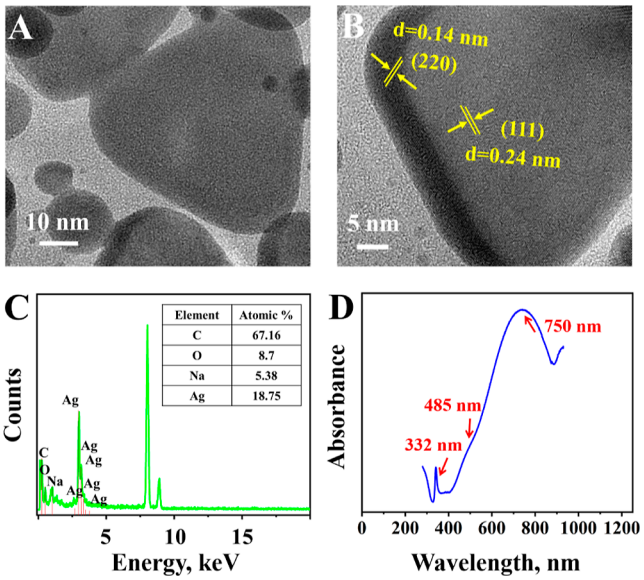

Figure 1. TEM (A) and HRTEM (B) images of Tri-Ag NPs$_{TSC}$. EDS (C) and UV−vis (D) images of Tri-Ag NPs$_{TSC}$, respectively.

(HRTEM) patterns depicted the glossy triangle-like morphology of the obtained Tri-Ag NPs$_{TSC}$ with an average length measured at ∼35 nm. After further magnification (Figure 1B), highly paralleled and ordered lattice fringes with a *d*-spacing of 0.14 and 0.24 nm are indexed to (111) and (220) faces, which corresponds to the abovementioned XRD results. Besides, the energy-dispersive X-ray spectrometry (EDS) spectra were applied to record the main elements of Tri-Ag NPs$_{TSC}$ including Ag, Na, O, and C (Figure 1C). As depicted in Figure 1D, the ultraviolet−visible (UV−vis) absorption spectra recorded three absorption peaks, representing out-of-plane quadrupole (332 nm), in-plane quadrupole (485 nm), and in-plane dipole plasmon resonance (750 nm) patterns of surface-confined TSC-capped Ag NPs.

Characterization of the Prepared ZMG Composites. It could be observed in the XRD patterns (Figure 2A) that the diffraction peaks of ZIF-67@MIL-88B combined the diffraction peaks of both MIL-88B and ZIF-67 with high crystallinity. Besides, the dark red color (ZIF-67@MIL-88B) indicated the successful embedding of MIL-88B nanorods (dark brown) in ZIF-67 polygonal crystals (light purple). The morphologies

https://doi.org/10.1021/acsami.2c05869
ACS Appl. Mater. Interfaces 2022, 14, 26271−26278

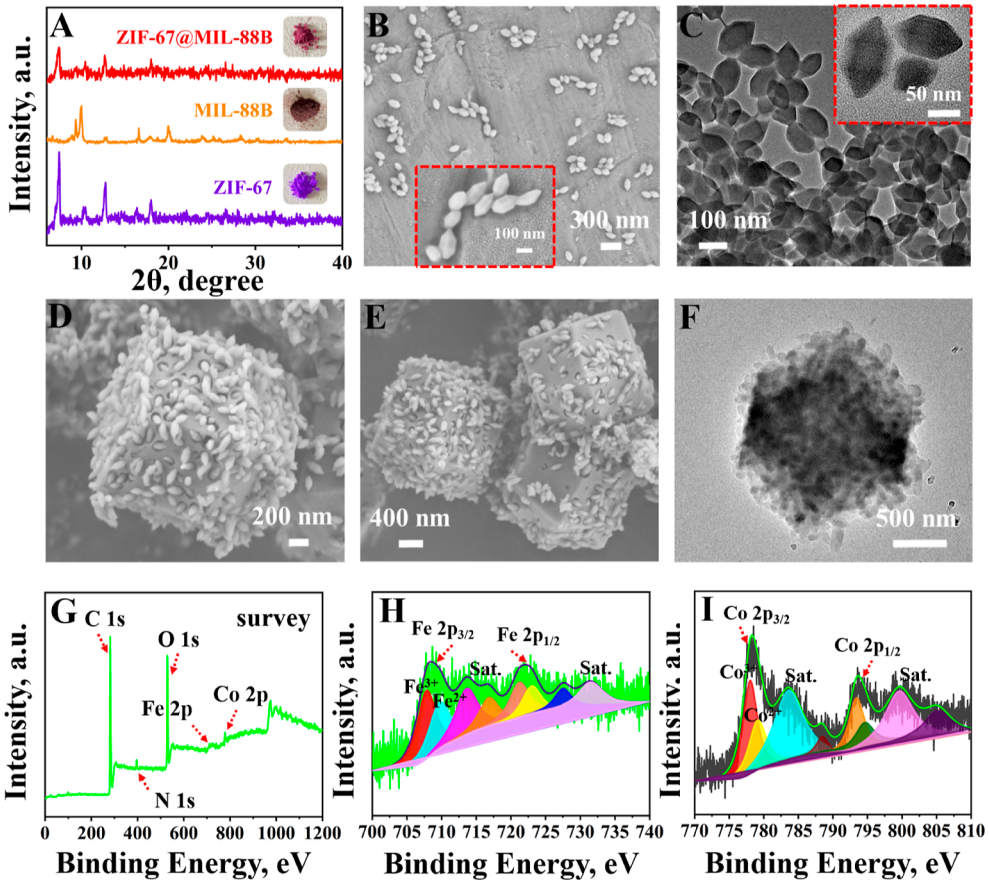

Figure 2. (A) XRD patterns and digital photographs (inset) of ZIF-67, MIL-88B, and ZIF-67@MIL-88B composites. (B) SEM and enlarged SEM images of MIL-88B. (C) TEM and enlarged TEM images of MIL-88B-GO_x. (D,E) SEM images of ZMG composites. (F) TEM image of ZMG composites. The XPS spectra of ZMG: (G) XPS survey spectrum of ZMG composites, (H,I) high-resolution XPS spectra of Fe 2p and Co 2p.

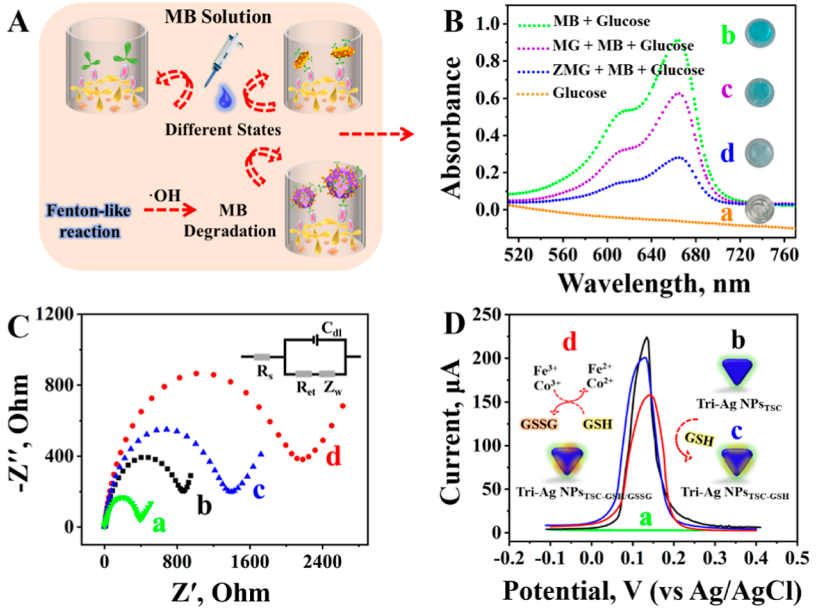

Figure 3. (A) Schematic of MB degradation under different states: labels blank, MG as the label, and ZMG as the label due to the generation of •OH in the presence of the glucose solution (1 mg/mL). (B) UV−vis spectrum of degraded MB under abovementioned different states. (C) EIS testing spectra and (D) DPV profiles of: (a) GCE/Nafion, (b) GCE/Tri-Ag NPs_{TSC}/Nafion, (c) GCE/Tri-Ag $NPs_{TSC-GSH}$/Nafion (with the adding of 8 μL of 500 pmol/L GSH), and (d) GCE/Tri-Ag $NPs_{TSC-GSH/GSSG}$/Nafion (upon a post-treatment with ZMG-based cascade reaction system oxidation, c_{AFB1} = 5 ng/mL).

https://doi.org/10.1021/acsami.2c05869
ACS Appl. Mater. Interfaces 2022, 14, 26271−26278

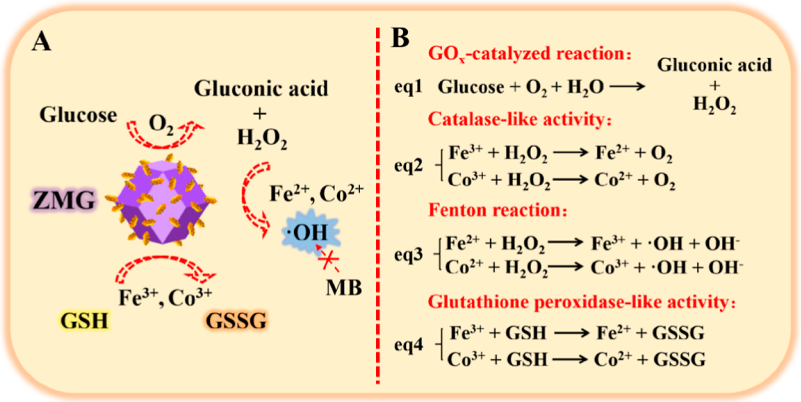

Figure 4. (A) Schematic diagram of the enzyme-like activities of ZMG. (B) Cascade reaction equations of the ZMG-based system.

and structures of MIL-88B, MIL-88B-GO_x, and ZMG composites were characterized by scanning electron microscopy (SEM) and TEM, respectively. It is clear that the equally distributed spindle-shaped MIL-88B with an average size of ~150 nm is observed in Figures 2B and S2A. The coordination between the $-NH_2$ and $-COOH$ groups of GO_x and the metal nodes of MIL-88B could adsorb GO_x to the surface of MIL-88B that obtained MIL-88B-GO_x. Apparently, there was almost no distinction in the morphology of fusiform MIL-88B after adsorption of the GO_x (Figures 2C and S2B). Moreover, SEM and TEM images (Figure 2D–F) exhibited the rugged ZMG polyhedron of uniform size (2–3 μm), which was prepared by embedding the randomly oriented MIL-88B-GO_x in ZIF-67. The existence and distribution of N, O, Fe, and Co in the ZMG composite was revealed by SEM elemental mapping images (Figure S3).

X-ray photoelectron spectroscopy (XPS) measurement was applied to identify the surface chemical valence states and elemental compositions of ZMG. As depicted in Figure 2G, the survey spectrum exhibited the main chemical composition of C, N, O, Fe, and Co, which is in accordance with the abovementioned EDS results. The high-resolution spectrum of Fe 2p (Figure 2H) involved two main peaks (Fe $2p_{3/2}$ and Fe $2p_{1/2}$) together with two satellite peaks. Especially, the binding energy of the Fe $2p_{3/2}$ peak located at 708.6 eV could be divided into two peaks that can be ascribed to the presence of Fe^{3+} (707.8 eV) and Fe^{2+} (709.7 eV) states in MIL-88B.[29] In the Co 2p spectrum (Figure 2I), two peaks (778.1 and 779.1 eV) which were spilt from the Co $2p_{3/2}$ peak are attributed to the Co^{2+} and Co^{3+} states, respectively.[20]

Characterization of $^{\bullet}OH$ Radicals by the MB Spectrophotometric Method. Referring to the work of Pang's group,[10] the GO_x of ZMG could effectively promote the decomposition of glucose to generate gluconic acid and H_2O_2. Furthermore, the presence of $^{\bullet}OH$, which is generated by the Fenton reaction, could be confirmed by the MB spectrophotometric method.[30] As depicted in Figure 3A, different specific status: labels blank, MG as the label (MG), and ZMG as the label (ZMG) were treated with the preparation procedure of 2.4, which was described above, respectively. Furthermore, 50 μL of the supernate was injected to a 96-well microplate by treating it with the same volume of the MB solution. After the degradation reaction, a UV–vis spectrum (Figure 3B) was applied to record the absorbance changes of the abovementioned mixtures. Apparently, the absorbance of MG (curve c) and ZMG (curve d) samples exhibited different degrees of decline compared with the labels blank sample (curve b), which could demonstrate the successful generation of $^{\bullet}OH$, and MB as a trapping agent could remove $^{\bullet}OH$. In particular, the lower obtained absorbance could prove that the ZMG sample exhibited a higher yield of $^{\bullet}OH$ than the MG sample. Meanwhile, the related color change could provide lateral proof of the abovementioned points.

EC Impedance Spectroscopy Characterization. Herein, the EC impedance spectroscopy (EIS) test (Figure 3C) was applied to explore the designed Tri-Ag $NPs_{TSC-GSH/GSSG}$ NRMs and characterize the assembly process of the proposed EC sensing interface.[31,32] It could be observed that the semicircle domain of GCE/Nafion (curve a), GCE/Tri-Ag NPs_{TSC}/Nafion (curve b), GCE/Tri-Ag $NPs_{TSC-GSH}$/Nafion (curve c), and GCE/Tri-Ag $NPs_{TSC-GSH/GSSG}$/Nafion (curve d) gradually expanded. Notably, there was an increase in the impedance of the Tri-Ag NPs_{TSC} after being partially replaced by GSH. It would be attributed to the electron transfer of Tri-Ag $NPs_{TSC-GSH}$ being blocked by thiols. Moreover, after partial GSH is transferred to oxidized GSSG, the GSH/GSSG surface mixed state of Tri-Ag $NPs_{TSC-GSH/GSSG}$ would further retard the electron transfer rate. Thus, a larger impedance increase of Tri-Ag $NPs_{TSC-GSH/GSSG}$ was obtained. Ultimately, abovementioned EIS results demonstrated the GCE/Tri-Ag $NPs_{TSC-GSH/GSSG}$/Nafion sensing interface was fabricated successfully. Table S1 illustrates the simulation parameters of the equivalent circuit components (Supporting Information).

Possible Mechanism of the Overall EC Biosensor. As for the signal-quenching mechanism, DPV signals (Figure 3D) of the surface-confined Tri-Ag NPs modified electrodes under different surface engineering status were compared, which is consistent with the EIS results. For GCE/Nafion (curve a), there was no DPV signal obtained. It was clear that after modifying with Tri-Ag NPs_{TSC}, a sharp and strong DPV profile was observed at around −0.13 V with the response value reaching about 220.4 μA (curve b). Whereas, owning to the hindrance of GSH (500 pmol/L) on electron transfer, the DPV response of Ag $NPs_{TSC-GSH}$ decreased to around 194.1 μA (curve c). Besides, a further decrease in the DPV signals of Tri-Ag $NPs_{TSC-GSH/GSSG}$ was obtained. Strikingly, Figure 4A,B presents the GSH peroxidase-like activity of ZMG together with the possible cascade reaction equations of the ZMG-based system. First, glucose could be catalyzed by GO_x to generate gluconic acid and H_2O_2 (eq 1). Subsequently, the ZMG would be partially decomposed by gluconic acid and release Fe^{3+} and Co^{3+} to react with H_2O_2 for Fe^{2+} and Co^{2+} generation (eq 2).

https://doi.org/10.1021/acsami.2c05869
ACS Appl. Mater. Interfaces 2022, 14, 26271–26278

Afterward, Fe^{2+} and Co^{2+} could transfer back to Fe^{3+} and Co^{3+} via the Fenton reaction in the presence of H_2O_2 (eq 3). The presence of $^{\bullet}OH$ was characterized by MB spectrophotometry, and MB was used to remove $^{\bullet}OH$ and prevent Tri-Ag NPs from being dissolved into Ag^{+}. Consequently, the obtained Fe^{3+}/Fe^{2+} and Co^{3+}/Co^{2+} with GSH peroxidase-like activity would oxidize GSH to GSSG (eq 4). It could be inferred that the ZMG-based system with various degrees of GSH peroxidase-like activity could convert partial GSH into disulfide oxidized GSSG. Hence, the formed GSH/GSSG surface mixed state would effectively hinder the oxidation process of Tri-Ag $NPs_{TSC-GSH/GSSG}$ that causes further signal quenching. Through this method, the error of this biosensor would be greatly avoided, thus improving the sensitivity.

Optimization of Experimental Conditions and AFB1 Analysis. Herein, several crucial parameters such as pH of the Tris-HCl buffer solution, concentration of the ZMG label, and electrode immersion time were investigated by monitoring the peak DPV responses (I_p) for optimal experimental conditions. First, the pH dependence of I_p was examined over pH values from 5.4 to 9.4 in a 0.1 mol/L Tris-HCl buffer solution (Figure S4). Clearly, the highest peak current, located at pH 7.4, could indicate it as the optimal pH value for further experiments. Besides, the concentration of the ZMG label could cause different GSH peroxidase-like activities of the ZMG-based cascade reaction system. As illustrated in Figure 5A, the

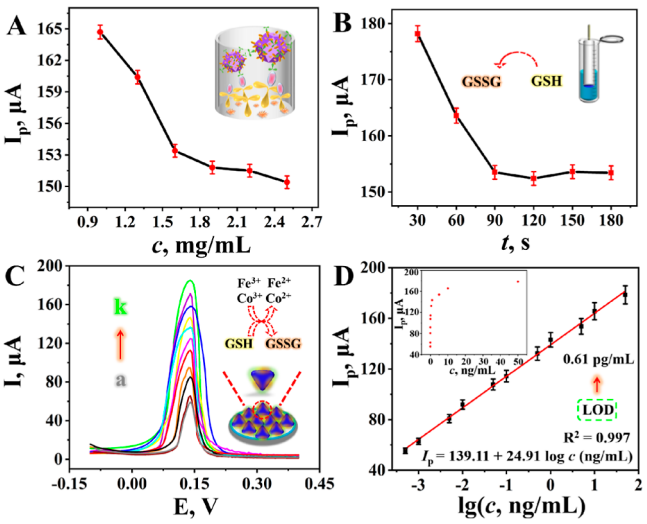

Figure 5. Optimization of experimental parameters: (A) effect of the ZMG label concentrations on the biosensor (incubated with 5 ng/mL AFB1). (B) Influence of immersion time of the ZMG-based solution on the Tri-Ag $NPs_{TSC-GSH}$-modified electrode. (C) DPV response profiles of the NRM-involved electrode with various concentrations of AFB1 from 500 fg/mL (curve a) to 50 ng/mL (curve k) acquired in a 0.1 mol/L Tris-HCl buffer solution (pH 7.4). (D) Corresponding linear calibration curve, linear equation, and LOD. Inset: calibration curve for AFB1 detection. Error bars = standard deviation (n = 3).

current decreased with the ZMG concentration up to 1.6 mg/mL. Subsequently, the significant slowdown in the decrease convinced 1.6 mg/mL was optimized as the optimal label concentration. Moreover, the immersion time of the Tri-Ag NP-involved electrode might play an important role during the surface engineering process of Tri-Ag NPs. Figure 5B presents when the immersion time came to 90 s, the downward trend of the tested I_p flattened out. The abovementioned phenomenon means that at this time, the GSH/GSSG ratio on the Tri-Ag NP surface has reached the optimal ratio, and the ΔI_p is the maximum. Thus, 90 s was optimized for preparing the surface-engineered Tri-Ag NPs.

By taking advantage of the designed high-performance Tri-Ag $NPs_{TSC-GSH/GSSG}$ as the NRMs, the proposed split-type EC biosensor was applied for the analysis of the AFB1 target. Under the optimal conditions, a series of the concentrations of the AFB1 antigen within the range from 0.0005 to 50 ng/mL were detected in this biosensor. It could be observed in Figure 5C, the DPV current presented an obvious upward trend with the increase of the concentration of AFB1. Notably, Figure 5D exhibits that the corresponding DPV response value is linearly related to the logarithm of AFB1 concentration, along with a calibration curve I_p = 24.91 log c_{AFB1} (ng/mL) + 139.11 (a correlation coefficient of 0.997). In addition, the developed Tri-Ag $NPs_{TSC-GSH/GSSG}$ NRM-based EC biosensor possesses a lower LOD calculated at 0.61 pg/mL (S/N = 3) in comparison with other means of analyzing the AFB1 (Table S2).

Performance Evaluation of the Proposed EC Biosensor and Its Application in Real Samples. As for the developed NRM-based EC biosensor, its acceptable, satisfying stability, reproducibility, and specificity were evaluated (Figure S5). Furthermore, a standard addition method through spiking the AFB1 target into the peanut sample was adopted. Pretreatment and dilution of peanut samples, and the ELISA analysis of AFB1 inherent concentration in peanut samples, are described in the Supporting Information. Concretely, by adding 0.05, 0.1, 0.5, and 5 ng/mL of AFB1 standard samples into the pre-handled peanut samples, four real samples were prepared for further analysis. As depicted in Table 1, the

Table 1. Analysis Results of Target AFB1 in the Peanut Sample Using the Proposed Tri-Ag $NPs_{TSC-GSH/GSSG}$-Involved EC Biosensor (the Concentration of Target AFB1 was Diluted into 0.325 ng/mL)

samples	addition contents (ng/mL)	detection contents (ng/mL)	RSD (%, n = 3)	recovery (%)
1	0.0500	0.376	3.5	102
2	0.100	0.425	3.0	100
3	0.500	0.822	4.1	99.4
4	5.00	5.27	4.4	98.9

recovery data of target AFB1 were obtained within the range of 98.9−102% along with relative standard deviation (RSD) in the scope of 3.03−4.38%. Consequently, abovementioned results indicated the convincing practicality and feasibility of this EC biosensor.

CONCLUSIONS

In this work, a surface-engineered Tri-Ag $NPs_{TSC-GSH/GSSG}$ as an efficient NRM was applied for a sensitive split-type EC bioassay. Concretely, partial GSH replacement and the latter ZMG-based cascade reaction system oxidation comprise the surface engineering process. Notably, the electron obstruction caused by the GSH/GSSG surface mixed state would initiate a dual signal-quenching mode that realizes sensitive changes in DPV response. Besides, by taking advantage of the split-type mode that separates specific recognition from EC determination, the impact of complex biological samples could be effectively avoided. Furthermore, the sensitivity and efficiency of the NRM-involved EC sensing interface have been greatly

https://doi.org/10.1021/acsami.2c05869
ACS Appl. Mater. Interfaces 2022, 14, 26271−26278

improved. Consequently, this proposed biosensor has been successfully applied to analyze the AFB1 target with admirable reproducibility, stability, and selectivity. All of the results could confirm the surface-engineered Tri-Ag $NPs_{TSC-GSH/GSSG}$ as a promising NRM to be applied for efficient NRM-based EC bioassay.

■ ASSOCIATED CONTENT

Supporting Information

The Supporting Information is available free of charge at https://pubs.acs.org/doi/10.1021/acsami.2c05869.

Materials and reagents; apparatus; synthesis process of PVP-functionalized MIL-88B-GO_x nanorods; characterization of materials including the XRD pattern of Tri-Ag NPs, TEM comparison images of MIL-88B and MIL-88B-GO_x nanorods and SEM mapping image of ZMG composites; pH optimization test of the Tris-HCl buffer solution; and EC performance analysis of this biosensor and other experimental details (PDF)

■ AUTHOR INFORMATION

Corresponding Author

Yu Du − *Collaborative Innovation Center for Green Chemical Manufacturing and Accurate Detection of Shandong Province, University of Jinan, Jinan 250022, P. R. China;* orcid.org/0000-0002-9002-8845; Email: duyu_ujn@163.com

Authors

Liu Qu − *Key Laboratory of Interfacial Reaction & Sensing Analysis in Universities of Shandong, School of Chemistry and Chemical Engineering, University of Jinan, Jinan 250022, P. R. China*

Jingshuai Li − *Key Laboratory of Interfacial Reaction & Sensing Analysis in Universities of Shandong, School of Chemistry and Chemical Engineering, University of Jinan, Jinan 250022, P. R. China*

Lei Yang − *Key Laboratory of Interfacial Reaction & Sensing Analysis in Universities of Shandong, School of Chemistry and Chemical Engineering, University of Jinan, Jinan 250022, P. R. China;* orcid.org/0000-0003-2153-3570

Xiang Ren − *Key Laboratory of Interfacial Reaction & Sensing Analysis in Universities of Shandong, School of Chemistry and Chemical Engineering, University of Jinan, Jinan 250022, P. R. China;* orcid.org/0000-0002-4321-4282

Lei Liu − *Key Laboratory of Interfacial Reaction & Sensing Analysis in Universities of Shandong, School of Chemistry and Chemical Engineering, University of Jinan, Jinan 250022, P. R. China*

Xuejing Liu − *Key Laboratory of Interfacial Reaction & Sensing Analysis in Universities of Shandong, School of Chemistry and Chemical Engineering, University of Jinan, Jinan 250022, P. R. China;* orcid.org/0000-0003-3644-0369

Yuyang Li − *Key Laboratory of Interfacial Reaction & Sensing Analysis in Universities of Shandong, School of Chemistry and Chemical Engineering, University of Jinan, Jinan 250022, P. R. China;* orcid.org/0000-0002-1399-9381

Qin Wei − *Key Laboratory of Interfacial Reaction & Sensing Analysis in Universities of Shandong, School of Chemistry and Chemical Engineering, University of Jinan, Jinan 250022, P. R. China;* orcid.org/0000-0002-3034-8046

Complete contact information is available at: https://pubs.acs.org/10.1021/acsami.2c05869

Author Contributions

[§]L.Q. and J.L. contributed equally to this work.

Notes

The authors declare no competing financial interest.

■ ACKNOWLEDGMENTS

This study was supported by the National Key Scientific Instrument and Equipment Development Project of China (no. 21627809) and the National Natural Science Foundation of China (no. 21777056). Q.W. thanks the Special Foundation for Taishan Scholar Professorship of Shandong Province, the Innovation Team Project of Colleges and Universities in Jinan (no. 2019GXRC027).

■ REFERENCES

(1) Wang, Y.; Wang, Y.; Wang, F.; Chi, H.; Zhao, G.; Zhang, Y.; Li, T.; Wei, Q. Electrochemical Aptasensor Based on Gold Modified Thiol Graphene as Sensing Platform and Gold-Palladium Modified Zirconium Metal-Organic Frameworks Nanozyme as Signal Enhancer for Ultrasensitive Detection of Mercury Ions. *J. Colloid Interface Sci.* **2022**, *606*, 510−517.

(2) Han, Y.; Qiu, C.; Li, J.; Gao, F.; Yuan, Q.; Tang, Y.; Niu, W.; Wang, X.; Gao, X.; Gao, L. Metal Cluster-Based Electrochemical Biosensing System for Detecting Epithelial-to-Mesenchymal Transition. *ACS Sens.* **2021**, *6*, 2290−2298.

(3) Qu, L.; Yang, L.; Li, Y.; Ren, X.; Wang, H.; Fan, D.; Wang, X.; Wei, Q.; Ju, H. Dual-Signaling Electrochemical Ratiometric Method for Competitive Immunoassay of CYFRA21-1 Based on Urchin-like Fe_3O_4@PDA-Ag and $Ni_3Si_2O_5(OH)_4$-Au Absorbed Methylene Blue Nanotubes. *ACS Appl. Mater. Interfaces* **2021**, *13*, 5795−5802.

(4) Hong, G.; Zou, Z.; Huang, Z.; Deng, H.; Chen, W.; Peng, H. Split-Type Electrochemiluminescent Gene Assay Platform Based on Gold Nanocluster Probe for Human Papillomavirus Diagnosis. *Biosens. Bioelectron.* **2021**, *178*, 113044.

(5) Zhang, J.; Gao, Y.; Zhang, X.; Feng, Q.; Zhan, C.; Song, J.; Zhang, W.; Song, W. Dual Signal-On" Split-Type Aptasensor for TNF-α: Integrating MQDs/ZIF-8@ZnO NR Arrays with MB-Liposome-Mediated Signal Amplification. *Anal. Chem.* **2021**, *93*, 7242−7249.

(6) Li, J.; Xu, L.; Shen, Y.; Guo, L.; Yin, H.; Fang, X.; Yang, Z.; Xu, Q.; Li, H. Superparamagnetic Nanostructures for Split-Type and Competitive-Mode Photoelectrochemical Aptasensing. *Anal. Chem.* **2020**, *92*, 8607−8613.

(7) Ma, N.; Ren, X.; Wang, H.; Kuang, X.; Fan, D.; Wu, D.; Wei, Q. Ultrasensitive Controlled Release Aptasensor Using Thymine-Hg^{2+}-Thymine Mismatch as a Molecular Switch for Hg^{2+} Detection. *Anal. Chem.* **2020**, *92*, 14069−14075.

(8) Chen, P.; Qiao, X.; Liu, J.; Xia, F.; Tian, D.; Zhou, C. Dual-Signaling Amplification Electrochemical Aptasensor Based on Hollow Polymeric Nanospheres for Acetamiprid Detection. *ACS Appl. Mater. Interfaces* **2019**, *11*, 14560−14566.

(9) Gao, X.; Dong, S.; Fu, L.; Zhang, B.; Hsu, H.-Y.; Zou, G. Use of Triangular Silver Nanoplates as Low Potential Redox Mediators for Electrochemical Sensing. *Anal. Chem.* **2021**, *93*, 3295−3300.

(10) Hu, C.; Wang, J.; Liu, S.; Cai, L.; Zhou, Y.; Liu, X.; Wang, M.; Liu, Z.; Pang, M. Urchin-Shaped Metal Organic/Hydrogen-Bonded Framework Nanocomposite as a Multifunctional Nanoreactor for Catalysis-Enhanced Synergetic Therapy. *ACS Appl. Mater. Interfaces* **2021**, *13*, 4825−4834.

(11) Li, H.; Wen, Y.; Zhu, X.; Wang, J.; Zhang, L.; Sun, B. Novel Heterostructure of a MXene@NiFe-LDH Nanohybrid with Superior Peroxidase-Like Activity for Sensitive Colorimetric Detection of Glutathione. *ACS Sustain. Chem. Eng.* **2020**, *8*, 520−526.

(12) Zhuo, X.; Henriksen-Lacey, M.; Jimenez de Aberasturi, D.; Sánchez-Iglesias, A.; Liz-Marzán, L. M. Shielded Silver Nanorods for Bioapplications. *Chem. Mater.* **2020**, *32*, 5879−5889.
(13) Tseng, E. N.; Hsiao, Y.-T.; Chen, Y.-C.; Chen, S.-Y.; Gloter, A.; Song, J.-M. Magnetism and Plasmonic Performance of Mesoscopic Hollow Ceria Spheres Decorated with Silver Nanoparticles. *Nanoscale* **2019**, *11*, 3574−3582.
(14) Chen, Y.; Tang, D.; Huang, Z.; Liu, X.; Chen, J.; Sekiguchi, T.; Qu, W.; Chen, J.; Xu, D.; Bando, Y.; Hu, X.; Wang, X.; Golberg, D.; Tang, X. Stable Single Atomic Silver Wires Assembling into a Circuitry-Connectable Nanoarray. *Nat. Commun.* **2021**, *12*, 1191.
(15) Wijaya, Y. N.; Kim, J.; Choi, W. M.; Park, S. H.; Kim, M. H. A Systematic Study of Triangular Silver Nanoplates: One-Pot Green Synthesis, Chemical Stability, and Sensing Application. *Nanoscale* **2017**, *9*, 11705−11712.
(16) Homan, K. A.; Souza, M.; Truby, R.; Luke, G. P.; Green, C.; Vreeland, E.; Emelianov, S. Silver Nanoplate Contrast Agents for in Vivo Molecular Photoacoustic Imaging. *ACS Nano* **2012**, *6*, 641−650.
(17) Muench, F.; Popovitz-Biro, R.; Bendikov, T.; Feldman, Y.; Hecker, B.; Oezaslan, M.; Rubinstein, I.; Vaskevich, A. Nucleation-Controlled Solution Deposition of Silver Nanoplate Architectures for Facile Derivatization and Catalytic Applications. *Adv. Mater.* **2018**, *30*, 1805179.
(18) Ardianrama, A. D.; Wijaya, Y. N.; Hur, S. H.; Woo, H.-C.; Kim, M. H. Reshaping of Triangular Silver Nanoplates by a Non-Halide Etchant and Its Application in Melamine Sensing. *J. Colloid Interface Sci.* **2019**, *552*, 485−493.
(19) Liu, S.; Tao, H.; Zeng, L.; Liu, Q.; Xu, Z.; Liu, Q.; Luo, J.-L. Shape-Dependent Electrocatalytic Reduction of CO_2 to CO on Triangular Silver Nanoplates. *J. Am. Chem. Soc.* **2017**, *139*, 2160−2163.
(20) Zhang, S. L.; Guan, B. Y.; Wu, H. B.; Lou, X. W. D. Metal-Organic Framework-Assisted Synthesis of Compact Fe_2O_3 Nanotubes in Co_3O_4 Host with Enhanced Lithium Storage Properties. *Nano-Micro Lett.* **2018**, *10*, 44.
(21) Li, X.; Du, Y.; Wang, H.; Ma, H.; Wu, D.; Ren, X.; Wei, Q.; Xu, J.-J. Self-Supply of H_2O_2 and O_2 by Hydrolyzing CaO_2 to Enhance the Electrochemiluminescence of Luminol Based on a Closed Bipolar Electrode. *Anal. Chem.* **2020**, *92*, 12693−12699.
(22) Feng, J.; Wang, H.; Ma, Z. Ultrasensitive Amperometric Immunosensor for the Prostate Specific Antigen by Exploiting a Fenton Reaction Induced by a Metal-Organic Framework Nanocomposite of Type Au/Fe-MOF with Peroxidase Mimicking Activity. *Microchim. Acta* **2020**, *187*, 95.
(23) Xu, W.; Jiao, L.; Yan, H.; Wu, Y.; Chen, L.; Gu, W.; Du, D.; Lin, Y.; Zhu, C. Glucose Oxidase-Integrated Metal-Organic Framework Hybrids as Biomimetic Cascade Nanozymes for Ultrasensitive Glucose Biosensing. *ACS Appl. Mater. Interfaces* **2019**, *11*, 22096−22101.
(24) Ma, J.-L.; Yin, B.-C.; Wu, X.; Ye, B.-C. Simple and Cost-Effective Glucose Detection Based on Carbon Nanodots Supported on Silver Nanoparticles. *Anal. Chem.* **2017**, *89*, 1323−1328.
(25) Xue, J.; Jia, Y.; Yang, L.; Feng, J.; Wu, D.; Ren, X.; Du, Y.; Ju, H.; Wei, Q. Etching Triangular Silver Nanoparticles by Self-generated Hydrogen Peroxide to Initiate the Response of an Electrochemiluminescence Sensing Platform. *Anal. Chem.* **2020**, *92*, 14203−14209.
(26) Gao, Y.; Zhang, J.; Zhang, X.; Li, J.; Zhang, R.; Song, W. Liposomal Controlled Release Ag-Activated DNAzyme Cycle Amplification on a 2D Pyrene COF-Based Photocathode for α-Synuclein Immunosensing. *Anal. Chem.* **2021**, *93*, 8647−8655.
(27) Wang, C.; Zhao, Q. A Reagentless Electrochemical Sensor for Aflatoxin B1 with Sensitive Signal-On Responses Using Aptamer with Methylene Blue Label at Specific Internal Thymine. *Biosens. Bioelectron.* **2020**, *167*, 112478.
(28) Wang, Q.; Zhao, F.; Yang, Q.; Wu, W. Graphene Oxide Quantum Dots Based Nanotree Illuminates AFB1: Dual Signal Amplified Aptasensor Detection AFB1. *Sens. Actuators, B* **2021**, *345*, 130387.
(29) Lu, Z.; Wang, K.; Cao, Y.; Li, Y.; Jia, D. Amino-Functionalized Iron-Based MOFs Modified with 2D $FeCo(OH)_x$ Hybrids for Boosting Oxygen Evolution. *J. Alloys Compd.* **2021**, *871*, 159580.
(30) Chang, M.; Wang, M.; Wang, M.; Shu, M.; Ding, B.; Li, C.; Pang, M.; Cui, S.; Hou, Z.; Lin, J. A Multifunctional Cascade Bioreactor Based on Hollow-Structured Cu_2MoS_4 for Synergetic Cancer Chemo-Dynamic Therapy/Starvation Therapy/Phototherapy/Immunotherapy with Remarkably Enhanced Efficacy. *Adv. Mater.* **2019**, *31*, 1905271.
(31) Qu, L.; Ren, X.; Fan, D.; Kuang, X.; Sun, X.; Wang, B.; Wei, Q.; Ju, H. Split-Type Electrochemical Immunoassay System Triggering Ascorbic Acid-Mediated Signal Magnification Based on a Controlled-Release Strategy. *ACS Appl. Mater. Interfaces* **2021**, *13*, 29179−29186.
(32) Xue, J.; Zhao, Q.; Yang, L.; Ma, H.; Wu, D.; Liu, L.; Ren, X.; Ju, H.; Wei, Q. Dual-Mode Sensing Platform Guided by Intramolecular Electrochemiluminescence of a Ruthenium Complex and Cationic N,N-Bis(2-(trimethylammonium iodide)propylene) Perylene-3,4,9,10-tetracarboxydiimide for Estradiol Assay. *Anal. Chem.* **2021**, *93*, 6088−6093.